Int. J. Electrochem. Sci., 4 **(2009)** 1063 - 1073

International Journal of ELECTROCHEMICAL SCIENCE
www.electrochemsci.org

Mesoporous Carbon Spheres: Synthesis, Characterization and Supercapacitance

*Jingxing Chen, Nannan Xia, Tianxiang Zhou, Sanxiang Tan, Fengping Jiang, Dingsheng Yuan**

Department of Chemistry, Jinan University, Guangzhou 510632, China
*E-mail: tydsh@jnu.edu.cn

Received: 27 May 2009 / *Accepted:* 14 August 2009 / *Published:* 25 August 2009

A green and efficient hydrothermal technique without any catalysts is used to prepare monodispersed carbon spheres from glucose for the potential supercapacitor application. As-prepared spherical carbon materials have been characterized by transmission electron microscopy, X-ray diffraction, N_2 adsorption, Fourier transition infrared spectroscopy and electrochemical techniques. After the activation treatment by molten KOH, mesoporous carbon spheres with ~2.2 nm mesopores, abundant hydrophilic functional groups and high specific surface area (1670 m^2 g^{-1}) have been obtained. Electrochemical characterization indicates a high specific capacitance (253 F g^{-1}) for such material. Further improvement in capacitance (302 F g^{-1}) is surprisingly found by introducing 10 wt% Pt onto mesoporous carbon spheres and a possible mechanism is proposed.

Keywords: Electric double-layer capacitors; Mesoporous carbon spheres; Specific capacitance

1. INTRODUCTION

Supercapacitors, as the complementary energy-storage devices of battery, have been intensively studied due to their long cycle life, highly reversible charge storage process and high specific power density. Supercapacitors are usually divided into two categories: the redox supercapacitor and electric double-layer capacitor (EDLC) [1]. Also known as pseudocapacitors, redox supercapacitors use redox reaction to produce a reversible Faradaic-type charge transfer and result in capacitance[2]. The pseudocapacitive materials generally include transition metal oxides such as RuO_2 [3], Bi_2O_3 [4] and MnO_2 [5] and conducting polymers such as polyaniline and polypyrrole [6, 7]. EDLC, similar to a conventional capacitor, stores charge electrostatically. However, it could store substantially more energy because the material used in it possesses high specific surface area and the

charge separation takes place across a very small distance in the electrical double layer that constitutes the interphase between an electrode and the adjacent electrolyte [1, 2].

The uniform and ordered carbon materials with high specific surface area and porous structure have been successfully applied to EDLCs [8-11]. Recently, owing to low fraction of microporous area and suitable pore size for EDLCs, the study on mesoporous carbon materials for supercapacitors has attracted a lot of attention [1, 6, 8]. Among various carbon materials, carbon spheres (CSs) are attractive candidates for functional materials due to their uniformity, high thermal stability, large packing density and excellent conductivity, and have been widely studied for various applications, such as adsorbent [12], catalyst support [13, 14] and anode in secondary lithium ion batteries [15]. Few literatures, however, have reported on mesoporous carbon spheres (MCSs) for supercapacitor application. CSs have been prepared by many synthesis routes using various carbon sources [16-22]. However, these synthesis methods either have low yield of CSs [16] or involve toxic / complicated processes [17, 21]. Alternatively, compared to these techniques, the hydrothermal method is one of the most efficient methods for carbon sphere synthesis and the synthetic route is very simple [23, 24].

Here, we report the synthesis of CSs via a hydrothermal route without the use of any toxic reagents or catalysts. Monodispersed MCSs have been obtained with activation and the yield of MCSs is more than 90 wt %. MCSs as electrode materials for EDLCs have been measured by electrochemical techniques and performed excellent supercapacitance. Subsequently, Pt nanoparticles have been loaded on the MCSs using the pulse-microwave assisted polyol method. In the process of methanol electrooxidation, surprisingly, we discover that Pt/ MCSs perform excellent capacitance. Pt/ MCSs are characterized for the application in electrochemical capacitor for the first time.

2. EXPERIMENTAL SECTION

All the chemical reagents in this work were of analytical grade purity, and used as-received. The 40g glucose was dissolved in the mixed solution containing 5mL ethanol and 40 mL distilled water and reacted in a stainless autoclave with 60 mL capacity for 10 h at 500~650 ^{o}C, and then allowed to cool to room temperature. The dark precipitate was collected and washed with absolute ethanol, distilled water and again with ethanol, then dried in vacuum at 80 ^{o}C for 6 h. CSs were further activated in molten KOH at 600 ^{o}C for 1 h prior to using as electrode materials. The Pt/MCSs were prepared by a pulse-microwave assisted polyol method. The primary steps of this synthesis process were given as follows: In a beaker, chloroplatinic acid as the starting precursor was well mixed with ethylene glycol in an ultrasonic bath, and then CSs were added into the mixture. After adjusted pH value of system more than 10 by the drop-wise addition of 1.0 mol L^{-1} NaOH / EG, the well-dispersed slurry was obtained with stirring and ultrasonication for 30 min. Thereafter, the slurry was microwave-heated in the form of pulse every 5 seconds for several times. In order to promote the adsorption of the suspended Pt nanoparticles onto the support, hydrochloric acid was adopted as the sedimentation promoter. The resulting black solid sample was filtered, washed and dried at 60 ^{o}C for 10 h in a vacuum oven.

Structural characterization of CSs and MCSs was performed using a MSAL-XD2 X-ray diffractometer (XRD) using Cu *K*α radiation (40kV, 20mA, λ=1.5406Å). The 2θ angular regions between 15 and 70 ^{o} were explored at a scan rate of 2 ^{o} min^{-1}. The morphology of as-product was carried out on a Philips XL30S scanning electron microscope (SEM, 20 kV) and transmission electron microscopic measurements were carried out on a JEOL TEM-2010 (HRTEM, 200 kV). The surface areas of CSs and the MCSs were measured via the Micromertics TriStar 3000 Analyzer. The functional groups of MCSs were detected by Nicolet 6700 FT-IR spectroscopy. The element contents of as-prepared Pt/MCSs composite were analyzed by an Oxford Inca 350 energy dispersive X-ray spectroscope (EDS). The valence of oxygen and platinum on Pt/MCSs and Pt/MCSs after electrochemical measurement (denoted as EO- Pt/MCSs) was characterized by X-ray photoelectron spectroscopy (Al *K*α, 200 W).

All electrochemical measurements were conducted on a CHI 660 B electrochemical workstation in a standard three-electrode cell at room temperature, adopting a saturated calomel electrode (SCE) and a platinum foil as the reference electrode and the counter electrode, respectively. A graphite disk was used as electrode substrate and was polished to a mirror-finish with 0.05 μm alumina suspension prior to each experiment. The thin film electroactive layer as the working electrode was prepared as follows: a mixture containing 3.0 mg as-prepared MCSs or Pt/MCSs, 0.9 mL ethanol and 0.1 mL Nafion solution (5 wt.%) were dispersed in an ultrasonic bar for 15 min to obtain a well-dispersed ink. The active material ink was then quantitatively transferred onto the surface of the graphite disk electrodes (d = 6mm) using a micropipette, and dried at 60 ^{o}C in oven to obtain a thin film. 0.5 mol L^{-1} H_2SO_4 was used as electrolyte solution.

3. RESULTS AND DISCUSSION

The monodispersed CSs were synthesized using only glucose as carbon source without any catalysts. We have investigated various factors affecting the preparation of CSs and the optimized synthesis condition was identified at 550 ^{o}C ~ 600 ^{o}C for 10h. The yield of the product is more than 90 % according to carbon weight percentage. SEM images of CSs and TEM images of the MCSs obtained under the optimum synthesis condition were shown in Fig. 1. The analysis of SEM presents that CSs with the diameter of 700~800 nm are uniform and monodisperse. According to TEM characterization, the as-prepared CSs show solid structure (see Fig. 1c). The enlarged magnification TEM image (Fig. 1d) reveals that the surface of CSs is rough after the activation treatment by molten KOH, probably due to the removal of amorphous carbons.

To compare the crystalline structure of MCSs with CSs, the X-ray diffraction (XRD) analysis was carried out and pattern of the as-prepared products are shown in Fig. 2. According to index JCPDS, No. 75-1621, the two peaks at 2θ = 25.9 ^{o} and 43.2 ^{o} are (002) and (101) diffraction planes of hexagonal graphitic carbon, respectively. A broad peak around 25.9 ^{o} indicates that the sample synthesized contains amorphous carbon. The diffraction peaks of MCSs are stronger than those of CSs and it proves that the graphitic degree of carbon materials increase after the activation treatment. The similar phenomenon had been observed in our previous report for another form of carbon material.

[25].

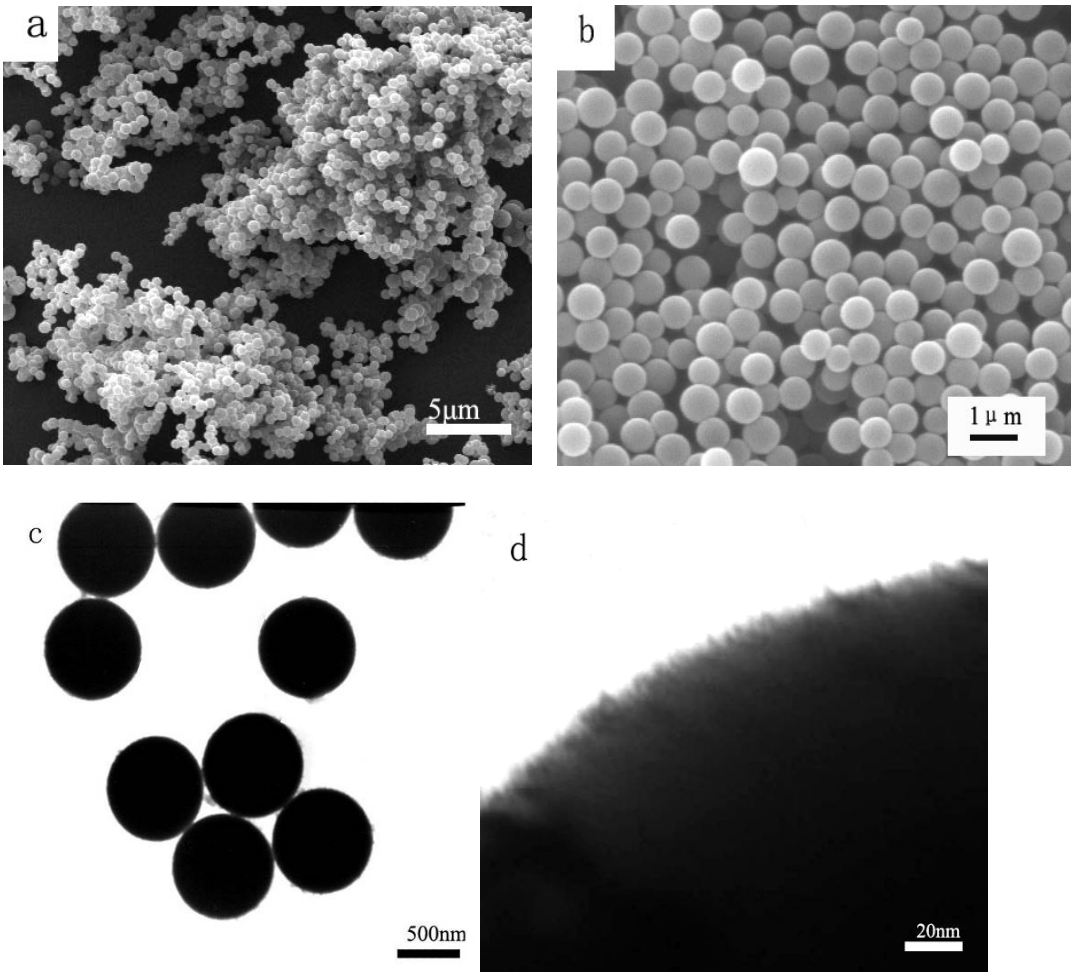

Fig. 1. SEM images of CSs synthesized by using glucose as carbon source at 550□ and TEM images of MCSs. (a) Low-magnification SEM image, (b) Enlarged magnification SEM image, (c) Low-magnification TEM image, (d) Enlarged magnification TEM image.

Besides removing amorphous carbons, activation treatment also results in the introduction of hydrophilic surface groups. The functional groups of MCSs were characterized by FT-IR, as shown in Fig. 3. The strong characteristic peak at 3428 cm^{-1} is attributed to the stretching vibration of O–H bond and the small peaks at 2921 and 2848 cm^{-1} originated from the stretching vibration of C–H bond. The peak at □1255 cm^{-1} corresponds to the stretching vibration of C-O bond. The infrared spectra peaks at 1590□1706 cm^{-1} are due to the stretching vibration of carboxyl groups C=O [26]. FT-IR spectrum confirms that there are many functional groups distributing on the surface of the MCSs. The retained functional groups provide a potential avenue to load other functional groups, molecules, metallic ions or nanoparticles [27].

The nitrogen adsorption–desorption isotherm of the MCSs is shown in Fig. 4. A type IV isotherm with a sharp capillary condensation step at high relative pressures (P/P_0 = 0.83 to 0.98) is observed and a hysteresis loop near relative pressure of 0.40□0.55 in the desorption branches indicates

the presence of mesopores. As shown in the inset of Fig. 4, a narrow pore size distribution (centered at ~2.2 nm) is calculated from the adsorption branch by the Barrett–Joyner–Halenda (BJH) method. The BET surface area of the MCSs is 1670 m^2 g^{-1} and 46 times more than that of CSs. The measurement results reveal that MCSs contain abundant mesopores.

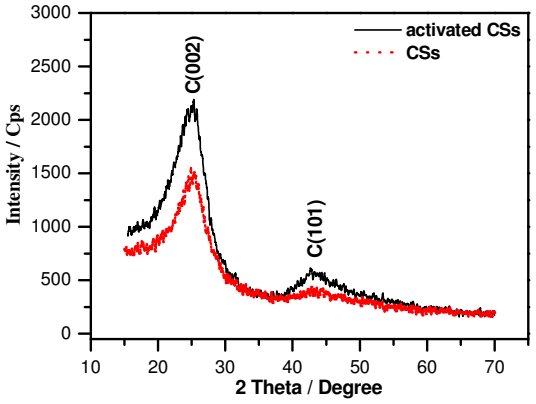

Fig. 2. XRD patterns of the as-prepared CSs and MCSs.

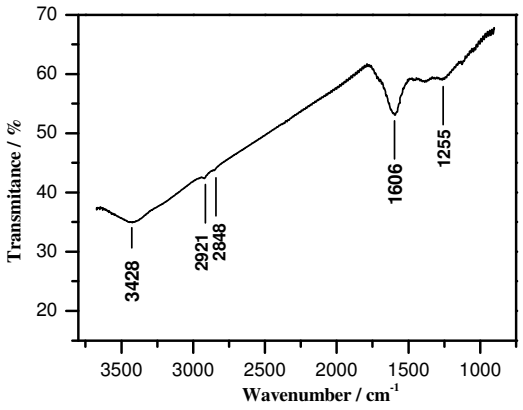

Fig. 3. FT-IR spectrum of the MCSs.

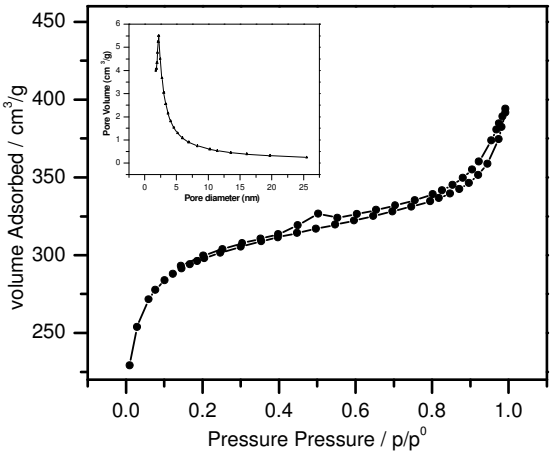

Fig. 4. Nitrogen adsorption-desorption isotherm of MCSs. The inset is the pore size distribution calculated by BJH method.

Based on their mesoporous structure and high BET surface area, MCSs could be a good candidate as electrode material for the supercapacitors. We have discovered a small quantity of Pt

nanoparticles loaded on MCSs to further improve its capacitance. To the best of our knowledge, this is the first report on using Pt / MCSs for electrochemical capacitor application. The morphology of the Pt/MCS is characterized by TEM. As shown in Fig. 5a, Pt nanoparticles with the diameter of 2~3 nm are uniformly dispersed onto the surface of MCSs. HRTEM image (Fig. 5b) shows Pt nanoparticles with the continuous lattice fringes with 0.20 nm spacing, corresponding to the spacing of (200) planes of Pt. The crystalline structure of loaded Pt is confirmed by the selected area electron diffraction (SAED) pattern (Fig. 5c), where the diffraction rings correspond to the (1 1 1), (2 0 0), (2 2 0), (3 1 1), and (2 2 2) facets of the face-centered cubic (fcc) structure. Fig. 5d shows an energy-dispersive spectrum (EDS) of as-prepared Pt / MCSs. The regular peaks at 2.1, 9.5 and 11 keV correspond to the signals of Pt K_α, Pt L_α and Pt L_β, respectively, highlighting the signature of metallic platinum (Pt^0) on MCSs surface. These are consistent with the literature about metallic Pt nanoparticles [28]. The typical loading of Pt nanoparticles on MCSs is 10 wt% by EDS analysis, in agreement with chemical synthesis.

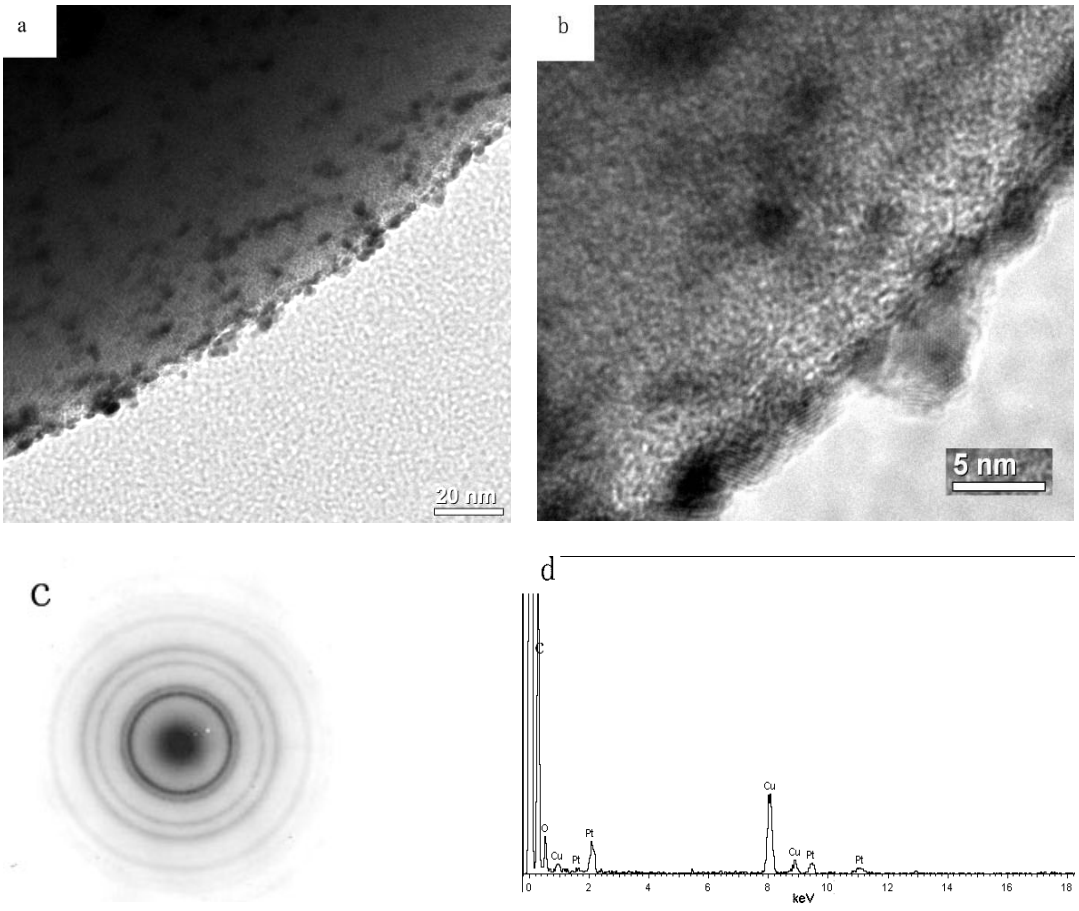

Fig. 5. TEM and EDS analysis of Pt/MCSs. (a) TEM image, (b) HRTEM image, (c) SAED and (d) EDS spectrum.

Cyclic voltammetry and galvanostatic technique are usually used to characterize the electrochemical capacitance of materials. Cyclic voltammetry is especially valuable and is the

preferred method for studying double-layer capacitor materials and resulting EDLC devices, since it provides detailed information directly on the double-layer capacitance and its potential dependence, which is essential for examining the behaviour and structure of electrified interfaces [9]. Fig. 6 shows the cyclic voltammograms (CVs) and charge-discharge curves of MCSs and Pt/MCSs. The specific capacitance of MCSs increases obviously after the loading of Pt, as shown in Fig. 6a. The slopes of current variation near the vertex potentials are almost vertical [7], indicating the good conductivity of MCSs and Pt/MCSs electrode. An ideal behavior of an EDLC should exhibit a rectangular shape on the voltammogram. However, a pair of reversible redox peaks is present in the range of 0.16□0.36 V (vs SCE) for both MCSs and Pt/MCSs. This could be explained by the functional groups on the carbon surface after the chemical activation treatment in molten KOH, as supported by the FT-IR experiment. Niu et al. also found the similar phenomenon where a weak maximum in both the anodic and cathodic current responses around 0.4-0.7 V (vs RHE) was observed [9]. Sullivan et al. explained that this is probably due to a pseudocapacitance contribution from surface functional groups, e.g. of the quinonoid type [29]. It causes an improvement of the specific capacitance through the psuedocapacitance effect via the following reactions [10, 11]:

$$\text{C-OH} \longleftrightarrow \text{>C=O} + H^+ + e^-$$
$$\text{-COOH} \longleftrightarrow \text{-COO}^- + H^+ + e^-$$
$$\text{> C=O + e-} \longleftrightarrow \text{> C-O}^-$$

The CVs of MCSs and Pt/MCSs for different sweep rate are shown in Fig. 6b and c. A voltammogram close to rectangular shape is obtained at slow sweep rate. This indicates the unrestricted motion of electrolytes in the pores at this slow sweep rate during the double-layer formation. With the increase of sweep rate, the voltammograms become tilted. This reflects that at fast sweep rates the ohmic resistance for electrolyte motion in carbon pores is significant and affects the double layer formation mechanism, in which the charge stored is recognized to be distributed [30, 2]. Increasing the sweep rate, the potential difference between the top and bottom of the pores becomes bigger, and thus results in the delayed current response as shown in the tilted voltammograms [8].

In cyclic voltammetry, current response, $i(V, t)$, at a sweep rate $\upsilon = d\,V / dt$, gives the double-layer capacitance, $C = i / \upsilon$. The dependence of Q on electrode potential (V), is then directly determinable as a differential quantity $C = d\,Q / d\,V$. Such quantities always give more resolved information than corresponding integral charging-curve relations, i.e. total charge *vs* potential. Hence, the specific capacitance C is directly and conveniently evaluated as a function of υ and potential by means of cyclic voltammetry [9] according to the following equation:

$$C = \frac{i}{m \times (d\mathrm{V} / dt)}$$

where i and m are the measured current and the mass of active carbon material, respectively. The data calculated from CVs of MCSs and Pt/MCSs are listed in Table 1. With increasing sweep rate, the

specific capacitance decreases and the introduction of Pt nanoparticles leads to the increase of the specific capacitance. The maximum *C* is 302 F g^{-1} for Pt/MCSs under low sweep rate of 5 mV s^{-1}.

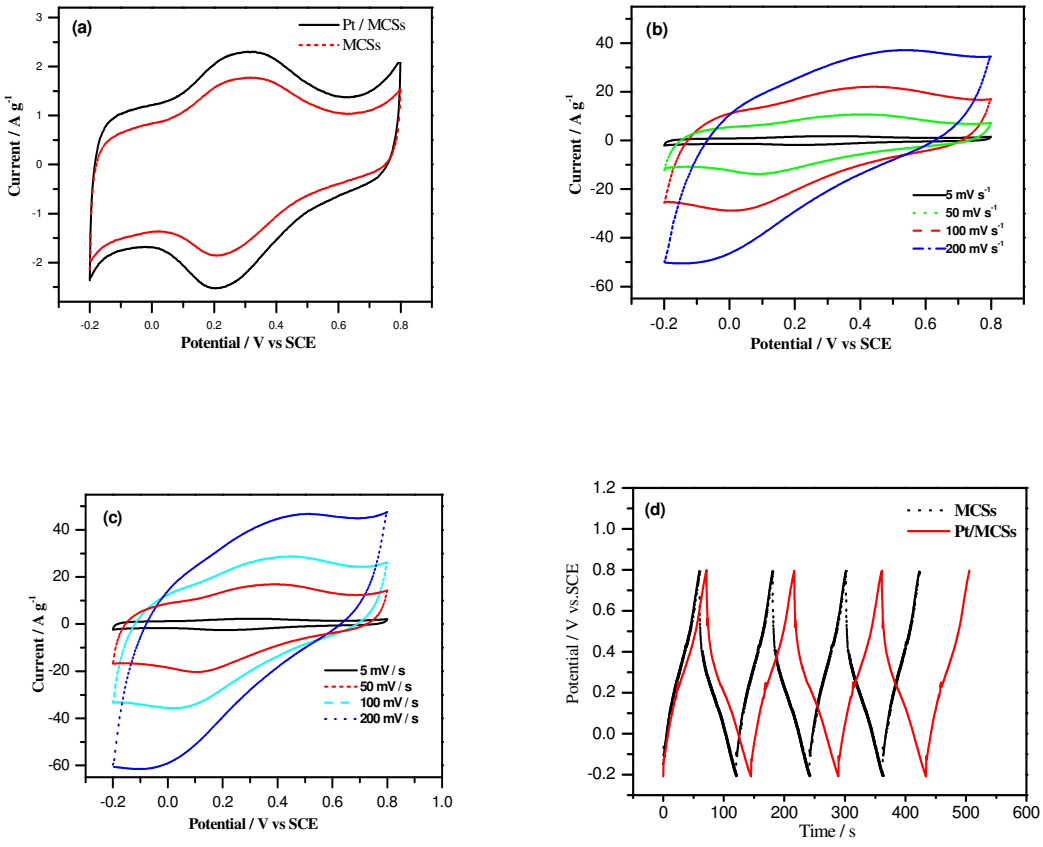

Fig. 6. Cyclic voltammograms and charge-discharge curves of MCSs and Pt/MCSs in 0.5 mol L^{-1} H_2SO_4 at room temperature. (a) CVs of MCSs and Pt/MCSs at sweep rate 5 mV s^{-1}. (b) CVs of MCSs at different sweep rates. (c) CVs of Pt/MCSs at different sweep rates. (d) charge-discharge curves of MCSs and Pt/MCSs at 4 A g^{-1}.

Table 1. Specific capacitances calculated from cyclic voltammograms at the MCSs and Pt/MCSs electrode in 0.5 mol L^{-1} H_2SO_4. (*C* : F g^{-1})

	5 mV s^{-1}	50 mV s^{-1}	100 mV s^{-1}	200 mV s^{-1}
MCSs	248	197	143	108
Pt/MCSs	302	227	188	141

To test the practical supercapacitance of carbon materials, the procedure of recording charge-discharge relations at constant-current is usually employed. The charge and discharge behaviours of the MCSs and Pt/MCSs were studied at 4, 8, 12, 16 and 25 A g^{-1} in 0.5 mol L^{-1} H_2SO_4. Typical charge-

discharge curves at 4 A g^{-1} are shown in Fig. 6d. The non-linearity between the potential and time indicates that the capacitance of the studied materials is not constant over the potential ranges both in charge and discharge cycle, as also confirmed by the CVs (see Fig. 7a). This variation could be due to the following reasons, including (a) the variation of the direct equivalent series resistance; (b) the redistribution of charges within the pores of the carbon material structure during charging or discharging; (c) any pseudocapacitance contribution due to redox-active surface groups [9]. From charge-discharge curves, the specific capacitance for active materials can also be calculated using:

$$C = \frac{it_d}{m\Delta V}$$

where i, t_d, m and ΔV are the constant current, discharging time, the mass of active materials and the total potential deviation, respectively. The calculated data for MCSs and Pt/MCSs are listed in Table 2. With higher charging current, the specific capacitance decreases and the maximum C reaches 297 F g^{-1} for Pt/MCSs at 4 A g^{-1}. Cycle life is also measured by conducting over 5000 times charge-discharge tests. Negligible changes in the curves were observed, revealing the excellent stability and reversibility of the as-prepared carbon materials.

Table 2. Specific capacitance calculated from charge-discharge curves at the MCSs and Pt/MCSs electrode in 0.5 mol L^{-1} H_2SO_4. (C : F g^{-1})

	4 A g^{-1}	8 A g^{-1}	12 A g^{-1}	16 A g^{-1}	25 A g^{-1}
MCSs	253	201	162	122	97
Pt/MCSs	297	256	238	223	183

Since both the double layer capacitance and pseudocapacitance are interfacial phenomena, basically, the high specific capacitance of MCS can be explained by its high specific surface area and the appropriately pore size (i.e. mesopores). On the other hand, the abundant functional groups contained in the MCS offer good wettability to the MCS surface and further enhance their charge storage capacity. [31]

After the introduction of Pt nanoparticles onto MCSs, the specific capacitance increases by 20% approximately. To elucidate the possible mechanism for such an increase, X-ray photoelectron spectroscopy (XPS) was conducted on Pt/MCSs. The XPS spectra of Pt/MCSs and electrochemically-oxidized Pt/MCSs (EO-Pt/MCSs) are shown in Fig. 7. From the comparison of curve 1 and curve 2 of the O1s spectra in Fig. 7a, a shoulder peak at a binding energy of 530.5 eV is more prominent for EO-Pt/MCSs. indicating the change of oxygen valence after electrochemical experiment. This shoulder peak is attributed to the formation of oxide Pt-O which necessitates the charge transfer from the Pt to the oxygen, and results in the formation of cationic Pt atoms and anionic oxygen. [31, 32] On the other hand, curve 1 in Fig. 7b reveals a shoulder peak at a binding energy of 75.6 eV, indicating the presence of Pt^{2+}. The positive shift in binding energy in the Pt 4f spectrum also suggests the formation of a strong Pt–O interaction.

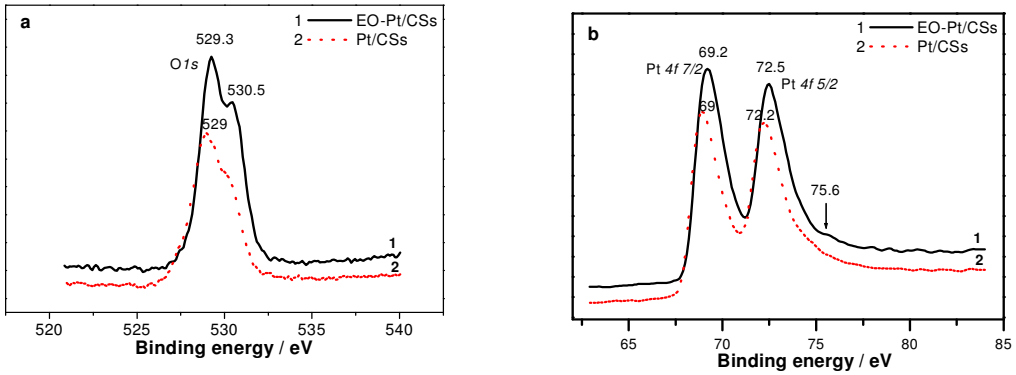

Fig. 7. XPS spectra of O 1s(a) and Pt 4f(b) for Pt/MCSs and EO-Pt/MCSs.

The difference in Pt 4f spectra suggests that the chemical state of the Pt atoms has changed before and after the electrochemical oxidation. The Pt surface oxidation seems a reasonable interpretation. Similar results had been reported in the literature [32]. The surface of nano-sized Pt is oxidized in the strong acid medium under high potential to form PtOH which is similar to RuO_2 with excellent supercapacitance. The tentative mechanism is proposed as follows:

$$Pt + H_2O \longleftrightarrow PtOH + H^+ + e^-$$

According to this reaction, the specific capacitance is estimated to increase by 49.5 F g^{-1} when 10 wt% Pt was loaded onto MCSs, which is consistent with the electrochemical measurement.

4. CONCLUSIONS

Monodisperse CSs with the diameter of 700-800 nm have been synthesized via a facile hydrothermal route using glucose as the carbon sources without using any catalysts. The MCSs with high specific surface area and abundant hydrophilic functional groups have been obtained by the treatment with molten KOH. Single electrodes of MCS materials exhibit high specific capacitance (253 F g^{-1}). Only 10 wt% Pt loading onto MCSs has been shown higher specific capacitance (302 F g^{-1}). The unique performance makes MCSs and Pt/MCSs potential candidates as electrode materials for supercapacitor.

ACKNOWLEDGMENTS
This work was financially supported by Natural Science Foundation of China (20876067) and the Young-teacher Fund of Jinan University (51208023).

References

1. A.G. Pandolfo and A. F. Hollenkamp, *J. Power Sources*, 157(2006)11

2. B.E. Conway, Electrochemical supercapacitors scientific fundamentals and technological application. New York: Kluwer/Plenum; 1999
3. J. H. Jang, K.J. Machida, Y.R. Kim and K. Naoi, *Electrochim. Acta*, 52(2006)1733
4. T.P. Gujar, V.R. Shinde, C.D. Lokhande and S.H. Han, *J. Power Sources*, 161(2006)1479
5. A.E. Fischer, K.A. Pettigrew, D.R. Rolison, R.M. Stroud and J.W. Long, *Nano. Lett*., 7(2007)281
6. Y.G. Wang, H.Q. Li and Y.Y. Xia, *Adv. Mater*., 18(2006)2619
7. J.H. Kim, Y.S. Lee, A. K. Sharma and C.G. Liu, *Electrochim. Acta*., 52(2006)1727
8. [H.Y. Liu, K.P. Wang and H. Teng, *Carbon*, 43(2005) 559
9. J.J. Niu, W.G. Pell and B.E. Conway, *J. Power Sources*, 156(2006) 725
10. S.W. Hwang and S.H. Hyun, *J. Non-Crystal. Solids*, 347(2004)238
11. E. Frackowiak, K. Metenier, V. Bertagna and F. Beguin, *Appl. Phys.Lett*., 77(2000)2421
12. Y. G. Wang, Y. Korai and I. Mocbida, *Carbon*, 37(1999)1049
13. C.W. Xu, L.Q. Cheng, P.K. Shen and Y.L. Liu, *Electrochem. Commun*., 9(2007)997
14. Y.C. Liu, X.P. Qiu, Y.Q. Huang and W.T. Zhu, *Carbon*, 40(2002)2375
15. R. Alcántara, F.J. Fernández Madrigal, P. Lavela, J.L. Tirado, J.M. Jiménez Mateos , C. Gómez de Salazar, R. Stoyanova and E. Zhecheva, *Carbon*, 38(2000)1031
16. H. Honda, H. Kimura, Y. Sanada, S. Sugawara and T. Furuta, *Carbon*, 8(1970)181
17. L.Q. Xu, W.Q. Zhang, Q. Yang, Y.W. Ding, W.C. Yu and Y.T. Qian, *Carbon*, 43(2005)1090
18. P. Serp, R. Feurer, P. Kalck, Y. Kihn, J.L. Faria and J.L. Figueiredo, *Carbon*, 39(2001)621
19. J.F. Yao, H.T. Wang, J. Liu, K.Y Chan, L.X. Zhang and N.P. Xu, *Carbon*, 43(2005)1709
20. T. Imamura, M. Nakamizo and H. Honda, *Carbon*, 16(1978)487
21. V.G. Pol, M. Motiei, A. Gedanken, J.C. Moreno and M. Yoshimura, *Carbon*, 42(2004)111
22. G. Hu, D. Ma, M.J. Cheng, L. Liu and X.H. Bao, *Chem. Commun*., 17(2002)1948
23. Q. Wang, H. Li, L. Q. Chen and X. J. Huang, *Carbon*, 39(2001)2211
24. D.S. Yuan, J.X. Chen, J.H. Zeng and S.X. Tan, *Electrochem. Commun*., 10(2008)1067
25. D.S. Yuan, S.Z. Tan, Y.L. Liu, J.H. Zeng, F.P. Hu, X. Wang and P.K. Shen. *Carbon*, 46(2008)531
26. C. Klinke, R. Kurt, J. M. Bonard and K. Kern, *J. Phys. Chem*. B, 106(2002)11191
27. A.M. Bond, W.J. Miao and C.L. Raston, *Langmuir*, 16(14) (2000)6004
28. B.R. Sathe, M.S. Risbud, S. Patil, K.S. Ajayakumar, R.C. Naik and I.S. Mulla, *Sensor Actuat.* A: *Phys*, 138(2)(2007)376
29. M.G. Sullivan, R. Kötz and O. Haas, *J. Electrochem. Soc*., 147(1) (2002)308
30. L.G. Austin and E.G. Gagnon, *J. Electrochem. Soc*., 120(2)(1973)251
31. V. Ganesh, S. Pitchumani and V. Lakshminarayanan, *J. Power Sources*, 158(2)(2006)1523
32. M.C. Jung, H.D. Kim, M. Han, W. Jo and D.C. Kim, *Jpn. J. Appl. Phys.*, 38(8)(1999)4872